Physicochem. Probl. Miner. Process., 55(1), 2019, 97-107

http://www.journalssystem.com/ppmp

Physicochemical Problems of Mineral Processing

ISSN 1643-1049

Received November 24, 2017; accepted April 11, 2018

The adsorption mechanism of Al(III) and Fe(III) ions on bastnaesite surfaces

Shiming Cao [1], Yijun Cao [2], Zilong Ma [2], Yinfei Liao [2]

[1] School of Chemical Engineering and Technology, China University of Mining and Technology, Xuzhou, China.

[2] National Engineering Research Center of Coal Preparation and Purification, China University of Mining and Technology, Xuzhou, China.

Corresponding author: yijuncao@126.com (Yijun Cao)

Abstract: The adsorption mechanism of Al(III) and Fe(III) ions on bastnaesite surfaces was investigated by a combination of DFT calculation, XPS analysis, adsorption isotherm study and adsorption kinetic investigations. DFT calculation results indicated that $\equiv CeOH^0$ and $\equiv CO_3H^0$ are primary functional groups on bastnaesite surfaces. XPS analysis reveals that Al(III) and Fe(III) ions adsorbed onto the bastnaesite surfaces through the interaction between aluminium/iron hydroxide species and oxygen atoms of surface $\equiv CeOH^0$ groups. No interaction between aluminium/iron hydroxide species and $\equiv CO_3H^0$ groups was detected. Adsorption isotherm studies demonstrated that the adsorption data of Al(III) and Fe(III) ions is fitted relatively well by Freundlich equations, the adsorption kinetic characteristics fitted to pseudo-second order model. Freundlich constants suggested favorable process for Al(III) and Fe(III) ions adsorption, and each adsorbed metal hydroxide specie complex with at least two oxygen atoms of surface $\equiv CeOH^0$ groups.

Keywords: Al(III), Fe(III), bastnaesite, adsorption

1. Introduction

As the development of advanced material and technology, the rare earths are more and more widely used in many fields, such as metallurgy, petrochemical industry, fine ceramics, luminescent materials and medical industry (Chi, 2014). The increasing demand of rare earth requires more effective rare earth mineral beneficiation. Bastnaesite is the primary light rare earth mineral, and floatation is one of the most important beneficiation methods for bastnaesite (Herrera-Urbina et al., 2013; Zhang, 2014).

In practical mineral flotation, ionic environment in solution is quite complicated. Bastnaesite and common gangue minerals such as calcite, fluorite, barite and celestite are all semisoluble minerals, in aqueous solution, a certain amount of ions would be dissolved into pulp. In practical mineral system, soluble salt minerals with much higher solubility may also exists. Fluid inclusions (Deng et al., 2013), mineral weathering and sliming can further increase the content and complexity of ions in pulp. These ions are referred to as "unavoidable ions". In addition, metal ions can be added as modifying agent. For example, aluminium salt is used as depressant in bastneasite separation from monazite (Ren and Song, 2000). The metal ions make non-ignorable changes in solution chemistry and mineral surface properties, and therefore affect bastnaesite beneficiation by flotation. Therefore, figuring out metal adsorption mechanism is fundamental to flotation, it provides foundation for solution control and mineral/water interface control.

In recent years, the adsorption mechanism of metal ions on mineral surfaces has been widely studied. Xu (2015) investigated the adsorption mechanism of Pb^{2+}on scheelite surfaces by flotation solution chemistry calculation and Zeta potential measurements. The results showed that $PbOH^+$ was dominated in adsorption at low pH, and adsorbed by precipitation of hydroxide at high pH. The adsorption of lead ions promoted collector adsorption, and therefore the scheelite floatation recovery was increased. Deng

DOI: 10.5277/ppmp18113

et al. (2017) found that the adsorption of Fe(III) on smithsonite surfaces is a complicated process, atomic composition and chemical state of smithsonite surfaces were changed. The results of solution chemistry calculation, XPS analysis and Zeta potential measurements suggested that Fe(III) adsorbed by chemical and electrostatic interactions. Feng et al. (2017) reported activation mechanism of lead ions in cassiterite flotation, the activation was attributed to hydrolyzed species $Pb0H^+$ in solution interacted with Sn-OH on the cassiterite surface to form the surface complex of Sn-O-Pb^+.Jia (2001) systematically studied the adsorption mechanism of Fe^{3+}, Cu^{2+}, Ni^{2+}, Zn^{2+}, Ca^{2+}, Pb^{2+} on six silicate minerals. The adsorption isotherm of each ion has been reported, and the isotherm equation of Kurbatov, Freundlich and Temkin was used for modeling equilibrium data, on this basis, the adsorption configuration of metal ions on mineral surfaces were discussed. The adsorption of 14 trivalent lanthanoid ions and yttrium ion on calcite surfaces was investigated by SAWADA, K. et al (SAWADA et al., 2005). The results showed that lanthanoids were adsorbed by competitive adsorption reactions of mono- and dihydroxo complexes. The heavy lanthanoid ions were primarily adsorbed as monohydroxo-complexes ($Ln(0H)^{2+}$), whereas the light lanthanoids were primarily adsorbed as dihydroxo-complexes($Ln(0H)_2^+$). However, despite these studies of metal ions adsorption mechanism on other minerals, the adsorption mechanism on bastnaesite surfaces has not been studied and minimal information is available in published literature.

In the present work, the functional groups on mineral surface, which plays a key role in adsorption was first discussed through crystal structure and broken bonds on mineral surfaces. The interaction between metal species and bastnaesite surfaces was investigated by solution chemistry and XPS. Finally, the adsorption configuration was confirmed by adsorption isotherm studies.

2. Materials and methods

2.1. Materials

Bastnaesite sample used in all the experiments was derived from Shandong province, China. The high grade raw ore was crushed and grinded to -1mm, then the grinding product was enriched by gravity separation and magnetic separation. Finally, bastnaesite sample with a purity above 95% was obtained. The X-ray diffraction (XRD) pattern of the representative sample is shown in Fig. 1.

Aluminium chloride ($AlCl_3 \cdot 6H_20$) and ferric chloride ($FeCl_3 \cdot 6H_20$) were supplied as aluminium-ion and iron-ion source, respectively. All reagents employed in the present study were of analytical grade, and pure deionized water was used throughout testing.

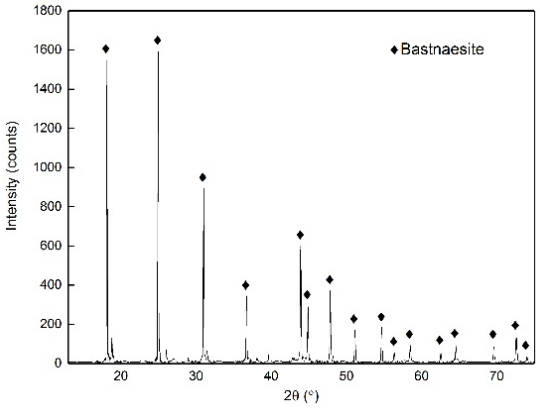

Fig. 1. XRD pattern of bastnaesite sample

2.2. Computational method and computational model

According to density functional theory (DFT), all calculations were performed using the CASTEP (Cambridge serial total energy package) program module. Valence electrons configuration considered in this study included Ce $4f^15d^16s^2$, F $2s^22p^5$, C $2s^22p^2$, O $2s^22p^4$ states. A plane-wave cut-off energy of 370 eV was used for all the calculation. The convergence tolerances for the geometry optimization calculations were set to a maximum displacement of 0.001 Å, a maximum force of 0.03 eV $Å^{-1}$, the

maximum energy change of 1×10^{-5} eV atom^{-1}, the maximum number of SCF cycles was 50 and 100 for geometry optimization calculation and energy calculation, respectively. Geometry optimization was conducted before energy calculation.

The crystal structure of bastnaesite $CeCO_3F$ is based on Ni, Y. et al. (Ni et al., 1953), and is shown in Fig. 2.

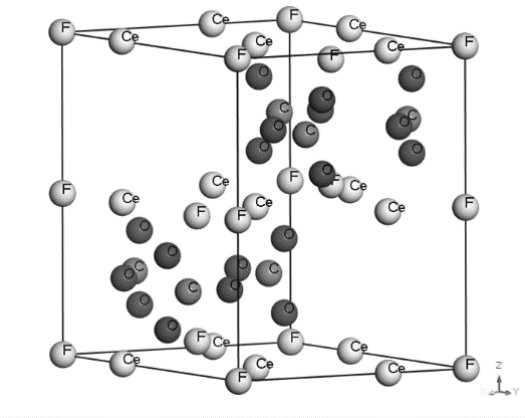

Fig. 2. Crystal structure of bastnaesite

2.3. Adsorption experiments

The adsorption experiments were conducted in a thermostatic water bath at 298K. Bastnaesite samples (1g) were dispersed in 40cm^3 of metal ion solution with various concentrations of 0.0-20.0mg/dm^3. The mineral suspensions were stirred for certain minutes, then the resultant suspension was subjected to solid–liquid separation using a centrifuge, and the separated liquid was collected to quantitatively analyze the metal ion concentration using an Inductively Coupled Plasma (ICP-OES, OPTIMA8300).

2.4. XPS analysis

XPS were conducted for three types of bastnaesite samples. One sample was treated without ions, and the other two were treated with Al(III)) and Fe(III) ions, respectively. Each sample was conditioned 40 min, and ion concentrations were both 1×10^{-4}mol/dm^3. The interaction products was examined via ESCALAB 250Xi with an Al K Alpha source. A survey scan of the analyzed sample was first conducted to detect elemental compositions, and then a precise scan was performed to obtain the XPS spectrum of a specific element. The C1s spectrum at 284.8 eV was obtained and used as an internal standard to calibrate all of the measured spectra for charge compensation.

3. Results and discussion

3.1. Functional groups of bastnaesite surfaces

Functional groups on mineral surface are the basic units in the interaction of ion adsorption in solution. In aqueous environment, metal species are adsorbed by complexing with surface functional groups, and past reports concluded that surface-complexed metal species widely present at aqueous/minerals interfaces (Parks, 1990; Wei and Wu, 2000; Wu, 2000; Nano and Strathmann, 2008).

The electron density of bastnaesite crystal is shown in Fig. 3a, it can be seen that the electron density changes along with different bonds. As shown in Fig. 3b there is great electron density in C-O region in carbonate groups, meaning that there is covalent interaction between C and O atoms, which is difficult to break in mineral liberation process. It can also be found that there is little electron density between O atoms and adjacent Ce atoms, which indicates an electrovalent bond which tends to break exists in Ce-O region. The electron density between Ce and adjacent F atoms is greater than that between Ce and O atoms (Fig. 3c, d), this implies that the Ce-F bond is more stable than Ce-O bond. It can also be found that there is no electron density in F-O region (Fig. 3d). According to bastnaesite crystal structure, there are alternating $(F\text{-}Ce)^{+II}$ and $(CO_3)^{-II}$ sheets, combined with electron density analysis, it can be deduced that the sheets are connected by electrovalent bond between Ce atoms in $(F\text{-}Ce)^{+II}$ sheet and O atoms in

$(CO_3)^{-II}$ sheet. From above discussion, it can be deduced that $\equiv F - Ce^{2+}$ and $\equiv CO_3^{2-}$ are the primary broken bonds exposed on bastnaesite surfaces during liberation.

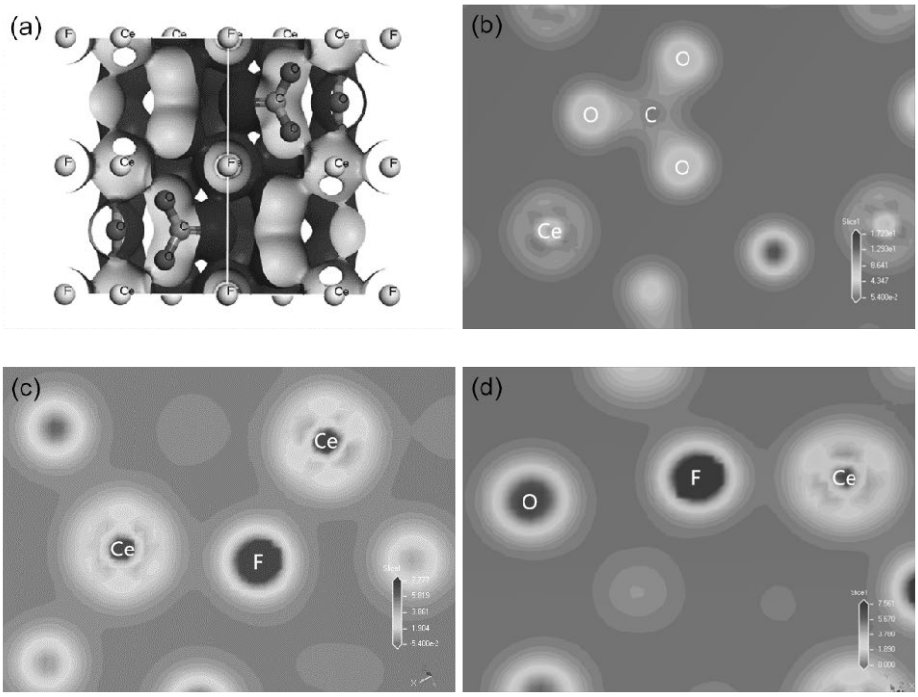

Fig 3. (a) Electron density of bastnaesite crystal, (b) Electron density maps between C-O and Ce-O atoms, (c) Electron density maps between Ce-F atoms, (d) Electron density maps between O-F and Ce-F atoms

According to the study of Zhang (2014), the bastnaesite in aqueous solution mainly present as Ce^{3+}, $CeFCO_3$, $CeCO_3^+$ and $Ce(CO_3)_2^-$, suggesting the bastnaesite surfaces showed the properties of intrinsic components instead of adsorbed precipitate such as $Ce(OH)_3$. In aqueous solution, the mineral surfaces interact with water molecules or other ions to counter the overcharge of breaking bonds. As a typical salt mineral, the surface cerium of $\equiv F - Ce^{2+}$ broken bonds complex with water molecules, referred as hydroxylation; and protonation takes place on anionic $\equiv CO_3^{2-}$ broken bonds. According to above discussion, the primary surface functional groups on bastnaesite surfaces in aqueous solution are $\equiv CeOH^0$ and $\equiv CO_3H^0$.

3.2. XPS analysis

XPS was used to identify the chemical compositions and chemical states of elements on the surfaces of bastnaesite samples. The XPS survey spectra of the original bastnaesite, the bastnaesite treated with aluminum ions and bastnaesite treated with iron ions within a binding energy of 1000-0 eV are shown in Fig. 4. It can be seen that in Fig. 4a, b and c, neither aluminum nor iron signal can be detected. But in the high-resolution XPS spectra for the bastnaesite treated with Al(III) ions and the bastnaesite treated with Fe(III) ions, Al and Fe can be detected. In Fig. 5a, the peak positioned at 74.65 eV of Al 2p is ascribed to adsorbed Al species on bastnaesite surfaces and it is consistent with the binding energy of aluminum hydroxide which is reported as 74.6 eV (HE et al., 1993), it implies that aluminum hydroxide may adsorb on bastnaesite surfaces. As shown Fig. 5b, the peak positioned at 710.65 eV of Fe 2p3 is assigned to adsorbed iron species on bastnaesite surface. The binding energy of Fe 2p3 is different with the standard spectrum of $FeCl_3$ which is reported as 711.2eV (Mullet et al., 2010), this finding indicates that iron hydroxide precipitated on bastnaesite surfaces (Deng et al., 2017).

As shown in Fig. 6a, the peak positioned at 684.65 eV is ascribed to F 1s of bastnaesite surfaces (Moulder et al., 1979; Cui et al., 2012). After treatment with Al(III) and Fe(III), the binding energy of F 1s is 684.7 eV and 684.75 eV (Fig. 6b, c), the chemical surroundings of F have not changed. Therefore, the F atom is not the adsorption site for Al(III) and Fe(III) ions.

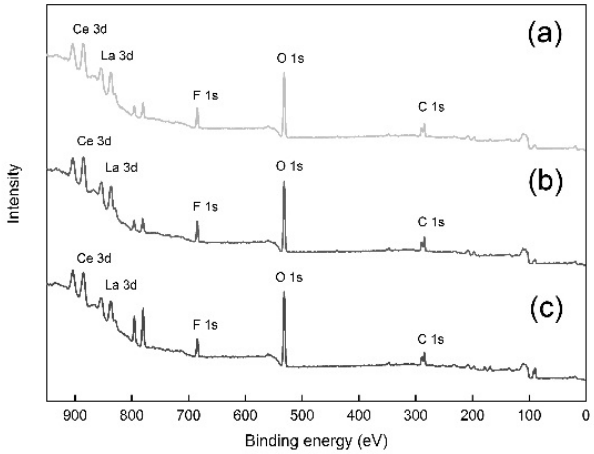

Fig. 4. XPS survey spectra of (a) untreated bastnaesite, (b) bastnaesite treated with aluminum ions, (c) bastnaesite treated with iron ions.

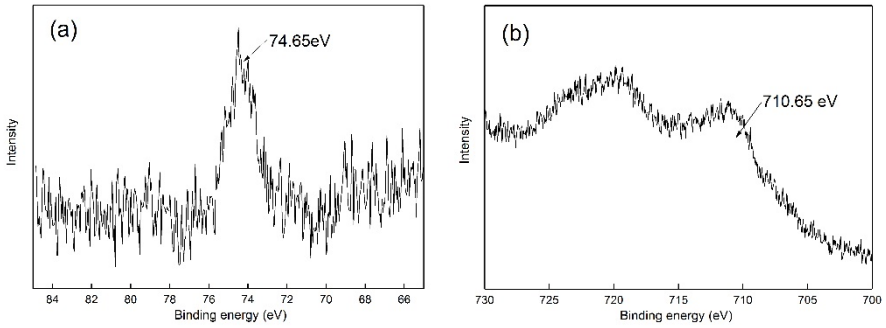

Fig. 5. (a) Al 2p spectra of the bastnaesite surfaces after aluminum ions treatment, (b) Fe 2p spectra of the bastnaesite surfaces after iron ions treatment

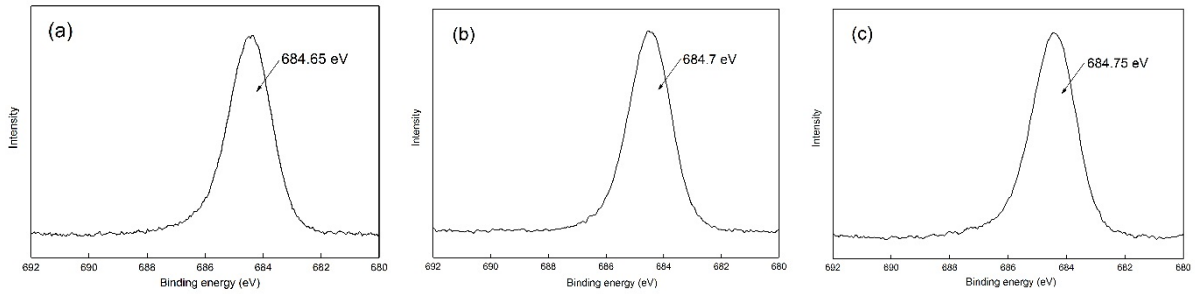

Fig. 6. F 1s spectra of (a) untreated bastnaesite, (b) bastnaesite treated with aluminum ions, and (c) bastnaesite treated with iron ions

The C 1s spectrum in Fig. 7a exhibits two well-separated peaks at 284.8 eV and 289.6 eV. The component at 284.8 eV is assigned to carbon contamination, while the peak at 289.6 eV is assigned to the C of CO_3^{2-} in bastnaesite (Moulder et al., 1979; Cui et al., 2012). As shown in Fig. 7b and Fig. 7c, after Al(III) and Fe(III) ions adsorption, the binding energy of C 1s in CO_3^{2-} is 289.55 eV and 289.6 eV, respectively. It indicates that the chemical surroundings of the C atom in the carbonate group have not changed.

As shown in Fig. 8a, the O 1s spectrum of the untreated bastnaesite can be fitted reasonably with two peaks at 531.57 eV and 532.3 eV. The O 1s peak positioned at 531.57eV was attributed to the oxygen in carbonate group of bastnaesite (Cui et al., 2012), and the other peak positioned at 532.3 eV was related to the oxygen in hydroxyl species ($\equiv CeOH^0$) (Moulder et al., 1979; Nowak et al., 2000; Feng et al., 2017). After the bastnaesite surface was modified by Al(III) and Fe(III) ions, the binding energy of O 1s in

carbonate group is 531.52 eV and 531.57 eV, respectively (Fig. 8b, c), meaning that the chemical surroundings of O atom in CO_3^{2-} of bastnaesite have not changed. Combined with binding energy analyze of C 1s in CO_3^{2-}, it can be concluded that the $\equiv CO_3H^0$ group on bastnaesite surface is not the adsorption site for Al(III) ions and Fe(III) ions.

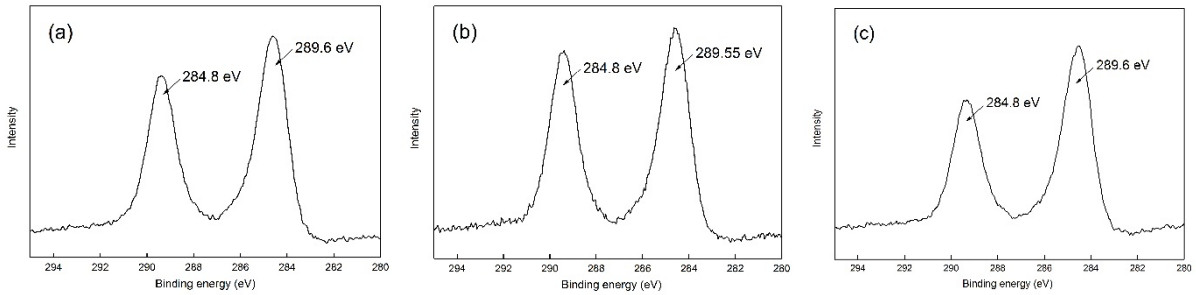

Fig. 7. C 1s spectra of (a) untreated bastnaesite, (b) bastnaesite treated with aluminum ions, and (c) bastnaesite treated with iron ions

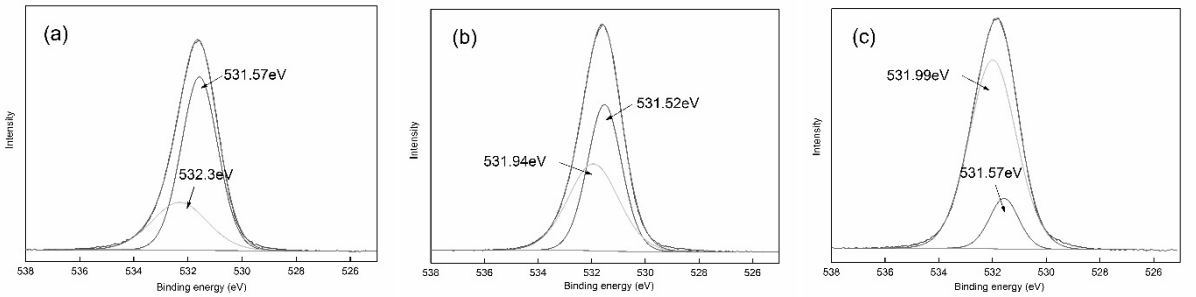

Fig. 8. O 1s spectra of (a) untreated bastnaesite, (b) bastnaesite treated with aluminum ions, and (c) bastnaesite treated with iron ions

Fig. 9 plots the diagrams of Al(III) and Fe(III) species distribution as a function of pH at the concentration of 1×10^{-4}mol/dm^3. The solution contains numerous aluminium/iron ion species, most of which are hydroxyl complexes. For aluminium ions (Fig. 9a), free Al^{3+} ions present at pH<5. $Al(OH)_3(aq)$ and $Al(OH)_3(s)$ appeared at about pH=4 and 4.1, and increased rapidly with pH; at pH>5, they become the main components. For iron ions (Fig. 9b), at pH>4, there are almost no free Fe^{3+} ions present. $FeOH^{2+}$ and $Fe(OH)_2^+$ mainly present at pH<5.5. At pH>6, the main components in solution are $Fe(OH)_3(aq)$ and $Fe(OH)_3(s)$.

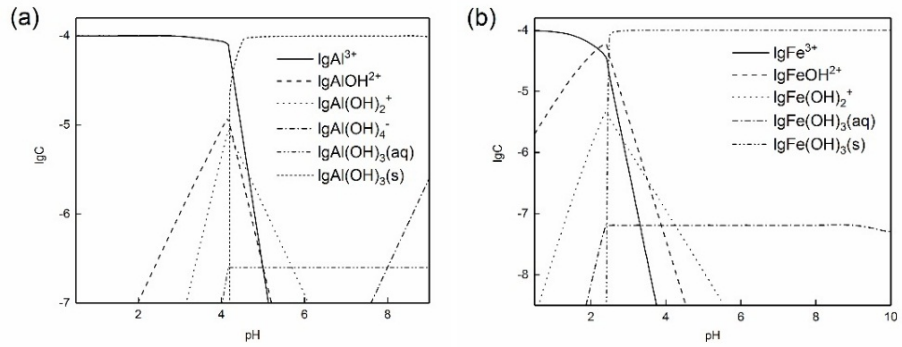

Fig. 9. (a) Distribution diagrams of Al(III) ions as a function of pH, (b) Distribution diagrams of Fe(III) ions as a function of pH

In alkalescency solution environment of XPS sample preparation, which is also the flotation pH environment, the aluminum ions and iron ions mainly present in the form of $Al(OH)_3(s)$, $Al(OH)_3(aq)$ and $Fe(OH)_3(s)$, $Fe(OH)_3(aq)$, hardly any free $Al^{3+}$and Fe^{3+} present in the solution, the formation of metal carbonate was consequently limited, therefore there is no interaction between ion species and

surface ≡ CO_3H^0 groups. In contrast, the binding energy of O 1s in hydroxyl species shifted by -0.36eV and -0.31eV respectively (Fig. 8b,c) after being treated with Al(III) ions and Fe(III) ions, it indicates that metal ion species may interact with the O atoms of surface ≡ $CeOH^0$ groups.

Fig. 10a shows the Ce 3d spectra of the original bastnaesite, and a double structure is obtained with a binding energy of 904.45 eV for the Ce 3d3/2 level and a binding energy of 885.85 eV for the Ce 3d5/2 level (Kotani and Ogasawara, 1992; Mullins et al., 1998; Cui et al., 2012). After treated with Al(III) ions, an obvious binding energy shift of Ce 3d3/2 and Ce 3d5/2 was observed. The binding energy of Ce 3d3/2 shifted by -0.35 eV and the binding energy of Ce 3d5/2 shifted by -0.45 eV. After treated with Fe(III) ions, the binding energy of Ce 3d3/2 shifted by -0.35 eV and the binding energy of Ce 3d5/2 shifted by -0.25 eV. The results indicate that the chemical surroundings of the Ce atom on bastnaesite surfaces have changed. By Combining with O1s binding energy analyze, it can be concluded that under the sample preparation pH, which is also the common flotation pH condition, the Al/Fe hydroxide adsorbed by interacting with ≡ $CeOH^0$ groups of bastnaesite surfaces.

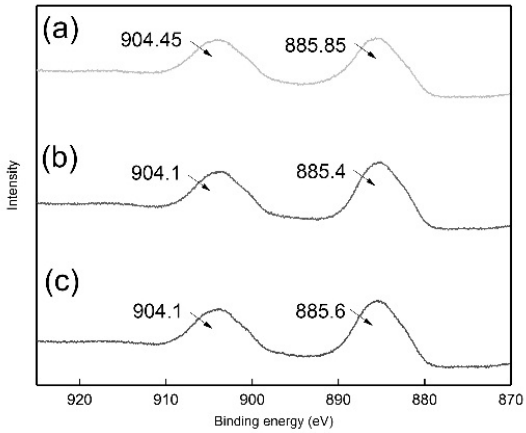

Fig. 10. Ce 3d3/2 and Ce 3d5/2 spectra of (a) untreated bastnaesite, (b) bastnaesite treated with aluminum ions, and (c) bastnaesite treated with iron ions

3.3. Adsorption isotherm and adsorption kinetic studies

Adsorption isotherms are used to study how adsorbates interact with the adsorbent materials. Three commonly used isotherm models, the Langmuir (Langmuir, 1918), Freundlich (Freundlich, 1915) and Temkin isotherms , are selected to analyze the equilibrium data for the adsorption of Al(III) and Fe(III) ions onto bastnaesite surfaces. The three models are given as follows:

$$\frac{1}{q_e} = \frac{1}{Q_0 k_l C_e} + \frac{1}{Q_0} \tag{1}$$

where C_e (mg/dm^3) is the equilibrium concentration of ions, q_e(mg/g) is the amount of ions adsorbed under equilibrium, k_l(dm^3/mg) is the Langmuir adsorption constant, and Q_0(mg/g) is the maximum adsorption amount.

$$\lg q_e = \lg k_F + \frac{1}{n}\lg C_e \tag{2}$$

where C_e (mg/dm^3) is the equilibrium concentration of ions, q_e(mg/g) is the amount of ions adsorbed under equilibrium, k_F and n are Freundlich constants, n giving an indication of how favorable the adsorption process and k_F (mg/g (dm^3/mg)$^{1/n}$) is the adsorption capacity of the adsorbent.

$$q_e = B\lg K_T + B\lg C_e \tag{3}$$

where C_e (mg/dm^3) is the equilibrium concentration of ions, q_e(mg/g) is the amount of ions adsorbed under equilibrium, B is related to the heat of adsorption and K_T(dm^3/mg) is the equilibrium binding constant.

The calculated parameters and correlation coefficient were listed in Table 1, and the resulting graphs are shown in Fig. 11. The assessment of data in Table 1 reveals that Freundlich model best fits the experimental adsorption data on account of the relative high regression (R^2) coefficient values obtained (R^2=0.96 for Al(III) adsorption and R^2=0.97 for Fe(III) adsorption). It must be noted that the R^2 of neither

Al(III) adsorption nor Fe(III) adsorption has achieved greater values (R^2>0.99), it implies that the ion adsorption mechanism is complicated, besides the interaction between metal hydroxide and surface $=CeOH^0$ groups, there may also be the precipitation of $Fe(OH)_3(s)$ on surfaces which formed in solution. The 1/n values calculated from the Freundlich model (0.49 and 0.19, respectively) were smaller than 1, showing that the Al(III) and Fe(III) ions could be readily adsorbed by bastnaesite at the temperature studied (CARTER, 1995). The Freundlich constant 1/n represents the number of metal ion species adsorbed by one adsorption site on mineral surface, therefore the n value represents the number of binding oxygen on mineral surface which one adsorbed ion specie interacted with (ZHOU and LI, 1996; WU et al., 1998; JIA, 2001). Through this the configuration of Al(III) and Fe(III) ions adsorption can be analyzed. The n value of Freundlich model for Al(III) and Fe(III) adsorption is 2.04 and 5.21, respectively, indicating that Al(III) and Fe(III) are adsorbed on bastnaesite surface by multicoordination, each adsorbed metal hydroxide specie complex with at least 2 oxygen atoms in $\equiv CeOH^0$ groups.

Table1 Isotherm model constants for Al(III) and Fe(III) adsorption onto bastnaesite surfaces (T = 298K)

Isotherm models	Constants	Al(III)	Fe(III)
Langmuir	Q_0	0.18	0.95
	k_l	0.05	12.90
	R^2	0.91	0.84
Freundlich	k_F	0.08	0.71
	n	2.04	5.21
	R^2	0.96	0.97
Temkin	K_T	8.89	263.53
	B	0.12	0.32
	R^2	0.90	0.91

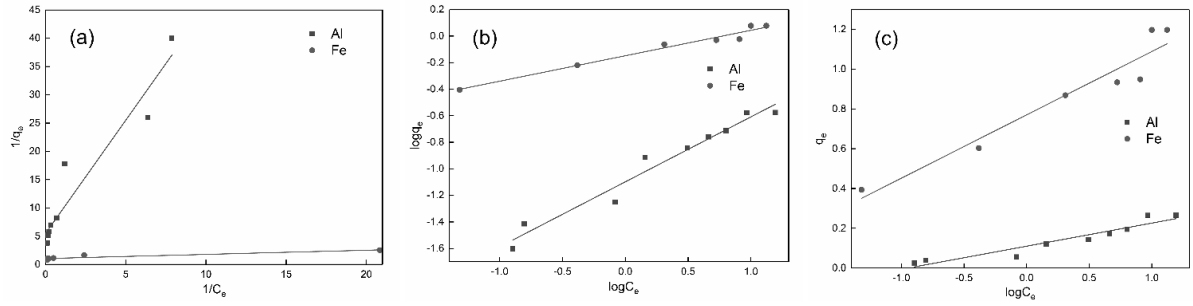

Fig. 11. Al(III) and Fe(III) ions adsorption of (a) Langmuir plots, (b) Freundlich and (c) Temkin plots

To further investigate how the Al(III) and Fe(III) ions in aqueous solution are adsorbed onto the bastnaesite surfaces, two widely used kinetics models, pseudo-first order and pseudo-second order (Ho and Mckay, 1999; Ho and Mckay, 1999) were examined to fit the experimental data. The linear expression of pseudo-first-order and pseudo-second-order models are expressed as follows:

$$\log(Q_{eq} - Q_t) = \log Q_{eq} - (\frac{K_1}{2.303})t \quad (4)$$

$$\frac{t}{Q_t} = \frac{1}{K_2 Q_{eq}^2} + \frac{t}{Q_{eq}} \quad (5)$$

where K_1 (min^{-1}) is the rate constant of the pseudo-first-order, K_2 (g/mg/min) is the second-order rate constant. Q_{eq} and Q_t (mg/g) are the adsorption capacities at equilibrium and time t (min), respectively. The calculated pseudo-first and second-order kinetic parameters and correlation coefficient were listed in Table 2, and corresponding kinetic plots are shown in Fig. 12. It can be seen that for both Al(III) and Fe(III) ions, the correlation coefficients of pseudo-second order kinetics were higher than 0.98, while the correlation coefficients of pseudo-first order kinetics were much lower. Therefore, pseudo-second order

kinetic model was considered more appropriate to represent the kinetic data. This tendency suggests that the adsorption progresses were mainly affected by chemical interactions, which is consistent with above-mentioned results, and the chemical interactions are attributed to the complexation between hydrolyzed species in solution with ≡ $CeOH^0$ groups on the bastnaesite surfaces to form the surface complex ≡Ce-O-Al/Fe-OH.

Table 2. Comparison of first and second order model for Al(III) and Fe(III) ions adsorption

Kinetic models	Constants	Al(III)	Fe(III)
Pseudo-first order	K_1	0.04	0.03
	Q_{eq}	0.21	0.29
	R^2	0.94	0.87
Pseudo-second order	K_2	0.49	0.47
	Q_{eq}	0.29	0.40
	R^2	0.99	0.99

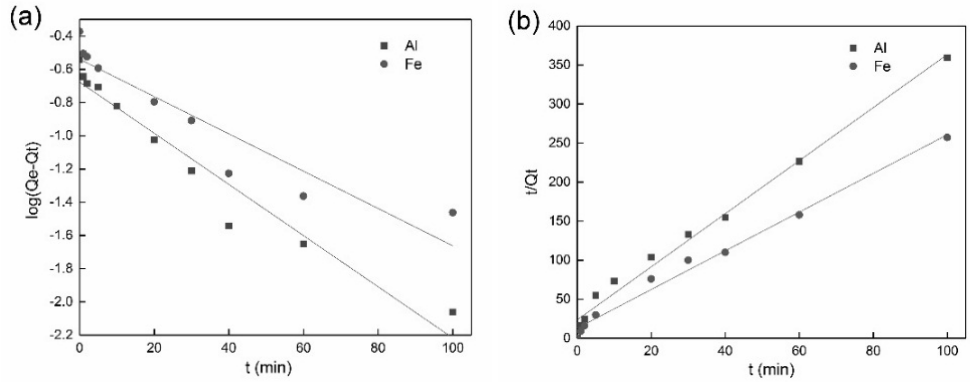

Fig. 12. Graphical representation of (a) the pseudo first order model and (b) the pseudo second order model

4. Conclusions

The present work examined the adsorption mechanism of Al(III) and Fe(III) ions on bastnaesite surfaces. Based on surface functional group study, XPS analysis and adsorption isotherm studies were conducted to understand the underlying mechanism. Given the abovementioned results, the primary conclusions are as follows:

1. In aqueous solution, the primary functional groups on bastnaesite surfaces are ≡ $CeOH^0$ and ≡ CO_3H^0.

2. ≡ CO_3H^0 groups and F sites on bastnaesite surfaces are not the adsorption sites for Al(III) and Fe(III) ions, the adsorption might be attributed to the interaction of hydrolyzed species in solution with ≡ $CeOH^0$ groups on the bastnaesite surfaces to form the surface complex ≡Ce-O-Al/Fe-OH.

3. Freundlich model best fits the experimental adsorption data of both aluminum and iron ions. Kinetic study further confirmed that the adsorption was mainly affected by chemical interaction. Analysis of Freundlich constants indicate that Al(III) and Fe(III) ions could be readily adsorbed by bastnaesite, and each adsorbed metal hydroxide specie interacts with at least 2 oxygen atoms of ≡ $CeOH^0$ groups.

According to the results of this study, the adsorption mechanism of Al(III) and Fe(III) ions on bastnaesite surfaces may be concluded as (Fig. 13):

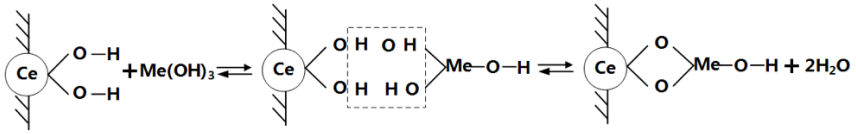

Fig. 13. Schematic representation of Al(III) and Fe(III) ions adsorption on bastnaesite surfaces (Me represents aluminum or iron ions)

Acknowledgments

This work was supported by Natural Science Foundation of China (51574240), the National Key Technology R&D Program for the 12th Five-Year Plan of China (No. 2014BAB01B05) and the Natural Science Foundation of Jiangsu Province (BK20150192).

References

CARTER, MC., KILDUFF, JE., WEBER, WJ., 1995. *Site energy distribution analysis of preloaded adsorbents.* Environ. Sci. Technol. 29(7), 1773.

CHI, R., WANG, D., 2014. *Mineral processing of rare earth minerals*. Science Press, Chap. 1.

CUI, J., HOPE, G A., Buckley, A N., 2012. *Spectroscopic investigation of the interaction of hydroxamate with bastnaesite (cerium) and rare earth oxides*. Miner. Eng. 36-38(5), 91-99.

DENG, J., WEN, S., XIAN, Y., LIU, J., BAI, S., 2013. *New discovery of unavoidable ions source in chalcopyrite flotation pulp: Fluid inclusions*. Miner. Eng. 42(3), 22-28.

DENG, R., HU, Y., KU, J., ZUO, W., YANG, Z., 2017. *Adsorption of Fe (III) on smithsonite surfaces and implications for flotation*. Colloid. Surface. A. 533, 308–315.

FENG, Q., ZHAO, W., WEN, S., CAO, Q., 2017. *Activation mechanism of lead ions in cassiterite flotation with salicylhydroxamic acid as collector*. Sep. Purif. Technol. 178, 193-199.

FREUNDLICH, HMF., 1915, *Uber die adsorption in lunsungen*. J. Phys. Chem. 57, 387-470.

HE, H., ALBERTI, K., BARR, T L., KLINOWSKI, J., 1993. *ESCA studies of aluminophosphate molecular sieves.* J. Phys. Chem. 97(51), 13703-13707.

HERRERA-URBINA, R., PRADIP, FUERSTENAU, D. W., 2013. *Electrophoretic mobility and computations of solid-aqueous solution equilibria for the bastnaesite-H2O system*. Miner. Metall. Proc. 30(1), 18-23.

HO, YS., MCKAY, G., 1999. *The sorption of lead(II) ions on peat.* Water. Res. 33(2), 578-584.

HO, YS., MCKAY, G., 1999. *Pseudo-second order model for sorption processes.* Process. Biochem. 34(5), 451-465.

JIA, M., 2001. *Surface structure study of silicate minerals and its adsorption mechanism for metal ions.* Northeastern University, 61-109.

KOTANI, A., OGASAWARA, H., 1992. *Theory of core-level spectroscopy of rare-earth oxides*. J. Elec. Spec. 60(4), 257-299.

LANGMUIR, I., 1918. *The adsorption of gases on plane surfaces of glass, mica and platinum*. J. Chem. Phys. 40(12), 1361-1403.

MOULDER, JF., CHASTAIN, J., KING, RCJ., 1979. *Handbook of x-ray photoelectron spectroscopy: a reference book of standard spectra for identification and interpretation of XPS data*. Chem. Phys. Lett. 220(1), 7-10.

MULLET, M., KHARE, V., RUBY, C., 2010. *XPS study of Fe(II) and Fe(III) (oxy)hydroxycarbonate green rust compounds*. Sur. Interf. Ana. 40(3-4), 323-328.

MULLINS, DR., HUNTLEY, DR., OVERBURY, SH., 1998. *Electron spectroscopy of single crystal and polycrystalline cerium oxide surfaces*. Surf. Sci. 409(2), 307-319.

NANO, GV., STRATHMANN, TJ., 2008. *Application of surface complexation modeling to the reactivity of iron (II) with nitroaromatic and oxime carbamate contaminants in aqueous TiO2 suspensions*. J. Colloid. Interf. Sci. 321(2), 350-359.

NI, Y., HUGHES, J.M., MARIANO, A.M., 1993. *The atomic arrangement of bastnasite-(Ce), Ce (C03) F, and structural elements of synchysite-(Ce), rontgenite-(Ce), and parisite-(Ce)*. Am. Mineral. 78, 415-418.

NOWAK, P., LAAJALEHTO, K., KARTIO, I., 2000. *A flotation related X-ray photoelectron spectroscopy study of the oxidation of galena surface.* Colloid. Surface. A. 161(3), 447-460.

PARKS, G.A., 1990. *Surface Energy and Adsorption at Mineral/Water Interfaces: An Introduction*. Set. Ana. 9(1-2), 1-2.

PIEROTTI, RA., SIEMIENIEWSKA, T., 1985. *Reporting physisorption data for gas/solid systems with special reference to the determination of surface area and porosity (Recommendations 1984)*. Pure. App. Chem. 57(4), 603-619.

REN, J., SONG, S., 2000. *Selective flotation of bastnaesite from monazite in rare earth concentrates using potassium alum as depressant*. Int. J. Miner. Process. 59(3), 237-245.

SAWADA, K., ABDEL-AAL, K., TAN, K., SATOH, K., 2005. *Adsorption of lanthanoid ions on calcite*. Dalton. T. 249(20), 3291-3296.

WEI, J., WU, D., 2000. *Ionize and complex reaction mode of mineral/water interface.* Adv. Eart. Sci. (01), 90-96.

WU, D., 2000. *Surface functional groups and surface reaction*. Geol. J. Chin. Un. (02), 225-232.

WU, H., WU, D., PENG, J., 1998. *Experimental study of the reaction between metal ions and quartz surface*. Geochemistry. (6), 521-531.

XU, H., 2015. *The adsorption mechanism of metal ions on scheelite surfaces and implications for flotation*. Jiangxi University of Science and Technology, 24-72.

ZHANG, X., 2014. *Surface chemistry aspects of fluorite and bastnaesite flotation systems*. The University of Utah, 100-102.

ZHOU, D., LI, X., 1996. *Adsorption characteristics of heavy metal ions onto soil in mass-action model*. J. Environ, Sci. 16(4), 425-430.